Non-weak inhibition and phase resetting at negative values of phase **in cells with fast-slow dynamics at hyperpolarized potentials**

Myongkeun Oh and Victor Matveev
Department of Mathematical Sciences and
Center for Applied Mathematics and Statistics
New Jersey Institute of Technology
Newark, NJ 07102

October 20, 2010

Abstract

Phase response is a powerful concept in the analysis of both weakly and non-weakly perturbed oscillators such as regularly spiking neurons, and is applicable if the oscillator returns to its limit cycle trajectory between successive perturbations. When the latter condition is violated, a formal application of the phase return map may yield phase values outside of its definition domain; in particular, strong synaptic inhibition may result in negative values of phase. The effect of a second perturbation arriving close to the first one is undetermined in this case. However, here we show that for a Morris-Lecar model of a spiking cell with **strong time scale separation**, extending the phase response function definition domain to an additional negative value branch allows to retain the accuracy of the phase response approach in the face of such strong inhibitory coupling. We use the resulting extended phase response function to accurately describe the response of a Morris-Lecar oscillator to consecutive non-weak synaptic inputs. This method is particularly useful when analyzing the dynamics of three or more non-weakly coupled cells, whereby more than one synaptic perturbation arrives per oscillation cycle into each cell. The method of perturbation prediction based on the negative-phase extension of the phase response function may be applicable to other excitable cell models **characterized by slow voltage dynamics at hyperpolarized potentials.**

1 Introduction

The phase response curve (PRC) proved to be a crucial mathematical concept in the study of perturbed oscillator dynamics, providing a very concise description of the response of an oscillator, for instance a regularly spiking neuron, to a synaptic input or other external perturbation (Winfree, 1974, 2001; Guckenheimer, 1975; Kuramoto, 1984). Whereas the infinitesimal PRC allows one to rigorously determine the effect of a weak synaptic input or perturbation of arbitrary duration under the assumption of linear summation of the perturbations arriving at different moments in time (reviewed in Izhikevich and Karamoto, 2006), the PRC approach is also applicable to non-weak inputs, whereby the linearity assumption does not hold, provided that the perturbation or synaptic input is brief, and that the perturbed cell returns to its limit cycle before receiving the next synaptic input or perturbation. In the latter case the PRC is referred to as the spike-time response curve (STRC) (Acker et al. 2003), and describes the change in the limit-cycle phase of the postsynaptic cell caused by the entire perturbation, as opposed to an infinitesimal brief pulse. The PRC/STRC approach proved extremely powerful for the description and analysis of synaptically coupled neuronal populations (Ermentrout and Kopell, 1984, 1990, 1991; Van Vreeswijk et al. 1994; Hansel et al. 1995; Canavier et al. 1997), including non-weakly coupled cells (Dror et al., 1999; Bressloff and Coombes, 2000; Acker et al. 2003; Netoff et al. 2003; Maran and Canavier, 2008; Canavier et al. 1999, 2009; Achuthan and Canavier, 2009; Canavier and Achuthan, 2010).

The crucial condition behind the phase response approach is the possibility of a one-dimensional reduction of the system state space along its limit cycle trajectory. In this case the phase variable (defined on the cyclical interval [0 1] or [0 2π]) gives full information about the position of the model along its periodic orbit, and therefore uniquely determines the time of occurrence of the next spike. Perturbation will shift the phase by the value of the phase resetting, delaying or advancing the next spike. However, a sufficiently strong perturbation may cause the trajectory to significantly deviate from the limit cycle, leading to the break-down of phase description. In the case of inhibition this happens for instance when the STRC delay $\Delta(\phi)$ received at phase ϕ satisfies $\Delta(\phi) > \phi$, formally causing the phase to become negative after the perturbation: $\phi_{new} = \phi_{old} - \Delta(\phi_{old}) < 0$, which reflects the fact that the next spike will arrive later than the unperturbed interval (we define phase resetting $\Delta(\phi)$ to be positive for a phase delay, and negative for a phase advance). Such negative values of phase arising from non-weak inhibition were first noted in the work of Canavier et al. (1999). In fact, Maran and Canavier (2008) demonstrated qualitatively new dynamical states such as stable "leap-frog" spiking (leader-switching) exhibited by two Wang-Buzsáki model neurons coupled by non-weak inhibition, which arise when phase variable is negative during part of each oscillation cycle. Recently we examined similar leader-switching in a homogeneous network of simpler Morris-Lecar model neurons pulse-coupled by non-weak inhibition (Oh and Matveev, 2009), and Canavier and coworkers further generalized the STRC approach to describe more complex phase-locked and clustered solutions in larger networks of non-weak coupled cells (Canavier et al. 2009; Achuthan and Canavier, 2009; Canavier and Achuthan, 2010).

In Oh and Matveev (2009) we analyzed stable leader-switching associated with the condition $\Delta(\phi) > \phi$, and demonstrated its geometric meaning in terms of isochrons that curl around the limit cycle, as shown in Figure 1. Namely, in this case the presynaptic cell at the peak of its action potential ($\phi_{pre} = 0$) has the ability to inhibit the postsynaptic cell onto an isochron which intersects the limit cycle at a phase that is retrograde to the peak of the action potential, and thus is negative, implementing the condition $\phi_{new} = \phi_{old} - \Delta(\phi_{old}) < 0$. This negative value of phase delays the postsynaptic cell enough to allow the presynaptic cell to bypass it along the limit cycle trajectory, reversing the spiking order of the two cells. We found that this isochron geometry is caused by the strong time-scale separation

Figure 1: (A) Effect of two consecutive synaptic perturbations in the Morris-Lecar model. When one of the cells reaches phase 0, corresponding to the peak of its potential ($\phi_{pre} = 0$), a synaptic current hyperpolarizes the postsynaptic cell, which has phase ϕ_{old} immediately preceding the input. If this first synaptic input (green arrow) is sufficiently strong, the resulting phase delay is greater than the phase difference between the two cells (i.e. $\Delta(\phi_{old}) > \phi_{old}$), and the new phase will be negative, $\phi_{new} = \phi_{old} - \Delta(\phi_{old}) < 0$. This negative phase corresponds to an isochron that intersects the limit cycle at a position retrograde to the peak of the action potential (red curve). If the next synaptic input arrives immediately after the first one (red arrow), the phase of the postsynaptic cell will still be negative, and the resulting phase delay will require the knowledge of the STRC at this hyperpolarized part of the trajectory, $\Delta(\phi_{new})$. Note that the two points lying on the same red isochron have values of phase that differ by one oscillation cycle, $\phi_{new} = \phi'_{new} - 1$, so while ϕ'_{new} is positive (and close to 1), the phase ϕ_{new} is negative. (B) Time scale separation in the ML model. Contour plot shows the ratio of the membrane potential time constant (a function of V and w) to the time constant of K channel activation (a function of V only). Contours are labeled with the ratio value; note that this ratio is smaller than 0.02 at hyperpolarized potentials. A limit cycle is superimposed on the contour plot (blue curve).

of the Morris-Lecar model in the parameter regime we consider, whereby the dynamics of the I_K activation gate (w) is much faster than the voltage dynamics at hyperpolarized potentials, making the w-nullcline a slow manifold of the system. In this case the portion of the w-nullcline at hyperpolarized values of voltage yields negative values of phase. While our prior study was aimed at elucidating the dynamical meaning of formally negative phase values, this work explores the possibility of defining STRC on such negative phase domain in order to predict a model cell's response to closely arriving non-weak perturbations.

Although the appearance of negative values of phase *between* perturbations does not violate the assumptions of the standard phase resetting approach, a qualitatively new situation arises in the case of two close synaptic inputs or perturbations, with the second perturbation arriving while the phase of the cell is still negative as a result of a strong delay caused by the first input. This scenario is described on the limit cycle plot in Figure 1, where the second input arrives immediately after the first one, so the phase of the postsynaptic cells is still negative, $\phi_{new} < 0$. In this case the return to the limit cycle trajectory could not have occurred between the two perturbations, violating the central assumption of the STRC approach. In general, full knowledge of the multi-dimensional state of the cell at the arrival time of the second input is required to predict the effect of this second perturbation. Alternatively, various approximations can be considered. For instance, Achuthan and Canavier (2009) use phase resetting at zero phase to describe the effect of perturbation received while the phase is negative. However, as we will show, the STRC method can be extended to this situation by defining and computing the value of the STRC along the negative branch of the phase domain. We find that this is indeed possible for biophysical models of excitable cells with strong time-scale separation, in particular the Morris-Lecar model (in a certain parameter regime, as discussed above). In fact, we will demonstrate that such an extended STRC approach enables accurate estimation of the effect of two or more close synaptic inputs. This approach can be applied to predict the dynamics of non-weakly coupled network of more than two cells, in which case several synaptic inputs in general arrive into each cell in each cycle of the oscillation, and with later inputs arriving before the cell relaxes to its regularly spiking trajectory (see Fig. 7).

Note that the existence of a unique value of STRC at negative phase values implies the existence of an approximate one-dimensional reduction of the state space of the cell in the relevant part of the perturbed trajectory outside of the limit cycle. As discussed above, in the case of the Morris-Lecar model such one-dimensional manifold consists of the limit cycle together with the portion of the w-nullcline that the system approaches after receiving a hyperpolarizing perturbation.

2 Methods

Regularly spiking cell model

We consider either a single or an all-to-all network of two or three identical Morris-Lecar model neurons (Morris and Lecar, 1981) with type-I excitability (Rinzel and Ermentrout, 1998), in the regime of strong time-scale separation (see Fig. 1). The differential equations for each model cell are

$$\begin{aligned} C\frac{dV}{dt} &= -I_{Ca} - I_K - I_L - I_{syn}(V,s) - I_{app} \\ \frac{dw}{dt} &= (w_\infty(V) - w)/\tau_\infty(V) \\ I_{Ca} &= \bar{g}_{Ca} m_\infty(V)(V - E_{Ca}) \\ I_K &= \bar{g}_K w(V)(V - E_K) \\ I_L &= \bar{g}_L(V - E_L) \end{aligned} \tag{1}$$

where $C = 2\ \mu F/cm^2$ is the membrane capacitance, V is the cell membrane voltage in mV, t is time in ms, I_L is the passive leak current, and $I_{app} = -14\mu A/cm^2$ is the applied current. The remaining parameters are $E_{Ca} = 120mV$, $E_K = -84mV$, $E_L = -60mV$, $g_{Ca} = 4mS/cm^2$, $g_K = 8mS/cm^2$, $g_L = 2mS/cm^2$.

The steady-state activation of calcium current is

$$m_\infty(V) = \frac{1}{2}\left[1 + \tanh\left(\frac{V+12}{18}\right)\right]$$

The potassium current activation amplitude and activation rate are

$$w_\infty(V) = \frac{1}{2}\left[1 + \tanh\left(\frac{V+8}{6}\right)\right]$$

$$\frac{1}{\tau_\infty(V)} = \frac{2}{3}\cosh\left[\frac{V+8}{12}\right]$$

The two cells are coupled through the synaptic current given by

$$I_{syn} = \bar{g}_{syn} s(t)(V - E_{inh})$$

where $\bar{g}_{syn}$ is the maximum synaptic conductance and $E_{inh} = -80mV$ is the reversal potential. The dynamics of the synaptic gating variable $s(t)$ depends on the presynaptic cell potential, V_{pre}:

$$\frac{ds}{dt} = -\frac{s}{\tau_{syn}}\sigma(V_{th} - V_{pre}) + \frac{1-s}{\tau_\gamma}\sigma(V_{pre} - V_{th})$$

where $V_{th} = -3$ mV is the synaptic threshold, $\sigma(\cdot)$ is a sigmoid function, $\sigma(x) = [1 + \tanh(4x)]/2$, and $\tau_{syn} = 1$ ms and $\tau_\gamma = 0.2$ ms are the synaptic decay and rising time constants, respectively.

Integration of this system of differential equations is carried out using MATLAB's (Mathworks, Inc) ode15s backward differentiation formula integrator.

Spike sequence prediction (emulation) using iterated phase map

In the last subsection of Results we use the iterated phase-map method described by Maran and Canavier (2008) and Achuthan and Canavier (2009) to compare the numerically simulated dynamics of an all-to-all coupled network of three Morris-Lecar model cell to the sequence of spikes obtained using the negative-phase STRC extension. However, we are using the voltage peak rather than spike threshold as the zero phase value, which changes slightly the phase map algorithm. Namely, the postsynaptic cells receive phase perturbation when the phase of the presynaptic cell reaches a value of 0.9945, which corresponds to the synaptic threshold potential and is slightly less than the value of 1^- corresponding to the peak of the spike. At this point the phases of the post-synaptic cells ϕ_j are updated by the value of their first-order phase resetting, $\Delta(\phi_j)$, while the value of the second-order phase resetting ($\Delta_2(\phi_j)$, red curve in Fig. 4B) is stored, to be used when the postsynaptic cell spikes. At the same point in time (e.g. when presynaptic cell phase reaches 0.9945), the phase of the presynaptic cell is reset to -0.0055, so that it crosses zero exactly at peak voltage, and any stored second-order phase resetting is subtracted from this reset value (see e.g. Canavier and Achuthan, 2010). Finally, it is important to check whether the presynaptic cell itself receives an input after it reaches synaptic threshold but before it reaches maximal potential. When this happens, only the second-order phase resetting is used to adjust the cell phase, since the first order phase-resetting is zero immediately preceding the peak voltage (see Fig. 4B). The fact that the phase of the presynaptic phase was "prematurely" reset causes no difficulty in the latter situation, since the spike-times are stored and checked independently of cell phases, so that appropriate second-order resetting can be properly computed.

3 Results

3.1 Negative phase and extended STRC for Quadratic Integrate-and-Fire model

In order to better illustrate the concept of negative phase, we first briefly discuss a simple example, the quadratic integrate-and-fire model, which represents a canonical model of a system with type-I excitability (Ermentrout and Kopell, 1986; Ermentrout, 1996; Latham et al., 2000). For our purposes it is important to consider a finite reset potential. In the super-threshold regime, the model can be non-dimensionalized in the form

$$\frac{dv}{dt} = v^2 + 1 \tag{2}$$

$$v(t_i^+) = v_r \tag{3}$$

where the spike times t_i are defined as points of divergence of $v(t)$, and v_r is the finite reset potential. Integrating this equation starting with the initial condition $v(0) = v_o$ yields (Hansel and Mato, 2003):

$$t = \arctan v(t) - \arctan v_0 \tag{4}$$

Setting $v_o = v_r$ and $v = \infty$ in the above equation yields the resting period of the cell:

$$T_0 = \frac{\pi}{2} - \arctan v_r \tag{5}$$

Normalizing Eq. 4 by the resting period defines phase as a function of voltage:

$$\phi(v) = (\arctan v - \arctan v_r)/T_0 \tag{6}$$

Figure 2: Phase resetting at negative phase values in the quadratic integrate-and-fire model with reset potential $v_r = -1$. (A) Double-branch phase geometry of the model. Negative phase values correspond to values of potential below the reset. (B) Phase response curve given by Eq. 8, for a hyperpolarizing pulse of amplitude $\delta v = -7$. The portion of the curve corresponding to negative phase values is shown in bold. **Negative phase values are bounded from below by $\phi_0 = -1/3$, since the passage time from $v = -\infty$ to $v = v_r$ is finite and equals $T_0/3$ for the chosen value of v_r.** (C) Response of the model cell to three consecutive hyperpolarizing pulses of equal amplitude. The three inputs arrive at times 0.2, 0.5 and 0.9 following the spike. The resulting perturbed inter-spike interval is completely determined by the values of phase response at three values of phase $\phi_{1,2,3}$ indicated in B; summing them yields a phase delay of $0.363 + 0.136 + 0.168 = 0.667$. Given the unperturbed period of 2.356, this corresponds to a time delay of 1.57 shown in this panel. (D) The evolution of phase variable corresponding to voltage trace in C.

Note that for values of potential below the reset value of v_r, the value of phase is negative, reflecting the fact that the time to spike (first passage time) is longer than the resting period T_0. Figure 2A illustrates the "tadpole"-like double-branch phase geometry of the integrate-and-fire model, noted by Golubitsky et al. (2006). The negative-phase interval is indispensable for parametrizing the state space of the model outside of the resting periodic trajectory, corresponding to the cyclic phase interval $[0, 1]$. Note finally that as the potential approaches $-\infty$, the phase approaches a finite minimal value $\phi_0 = (-\pi/2 - \arctan v_r)/T_0$, indicating finite-time divergence in backward time. In Figure 2B we set $v_r = -1$, so the negative phase domain extends down to $\phi_0 = -1/3$.

The phase resetting (delay) due to instantaneous hyperpolarization of amplitude δv can now be easily computed from the above expression:

$$\Delta(\phi) \equiv \phi(v) - \phi(v - \delta v) = \frac{\arctan v - \arctan(v - \delta v)}{T_0} \tag{7}$$

where the dependence on phase is defined implicitly by Eq. 6 (note that $\phi(v)$ is monotonic), yielding the phase response function shown in Figure 2B (Izhikevich, 2006):

$$\Delta(\phi) = \phi + \frac{\arctan v_r - \arctan(\ \tan(\ T_0\ \phi\ +\ \arctan v_r) - \delta v)}{T_0} \tag{8}$$

Note that this expression describes phase response to finite-strength perturbation, and is not proportional to the infinitesimal phase response curve (Ermentrout, 1996; Pfeuty et al., 2003). Figure 2B shows the phase resetting for the case $v_r = -1$.

The response of the model neuron to any sequence of instantaneous perturbations of given amplitude is completely described by the above phase resetting function, as shown in Figure 2C for the case of three perturbations. The total phase delay due to all three inputs is a sum of phase response values indicated in panel B. Here ϕ_1 is the cell phase at time of arrival of the first input, while the second and third inputs arrive at phases

$$\phi_2 = \phi_1 - \Delta(\phi_1) + \Delta t_1/T_0 \tag{9}$$

$$\phi_3 = \phi_2 - \Delta(\phi_2) + \Delta t_2/T_0 \tag{10}$$

where $T_0 = 2.356$ is the unperturbed period, $\Delta(\phi_{1,2})$ are the phase delays at phases $\phi_{1,2}$, and $\Delta t_{1,2}$ are the time intervals between consecutive synaptic currents. Note that the latter two inputs arrive when the potential of the cell is below reset, i.e. when the cell phase is negative (see panel D), demonstrating the utility of negative-phase extension of the phase response curve.

For time-dependent perturbations of arbitrary time course (for example, model synaptic currents) the phase resetting function in general cannot be analytically calculated, but can be computed numerically (as we do below for the case of the Morris-Lecar model, Fig. 4B). The resulting STRC will completely characterize the model response to time-dependent perturbations, provided that the time between inputs is larger than the duration of each perturbation.

Although the above negative-phase generalization of the phase response function is straightforward in the case of a one-dimensional model system, the main goal of this study is to explore the possibility of performing a similar negative-phase extension in the case of more biophysically-grounded conductance-based model, given a sufficient time-scale separation characterizing its dynamics.

3.2 Defining negative phase and extended STRC in the Morris-Lecar model

We now consider the Morris-Lecar model in the same type-I excitability parameter regime as in our previous work (Oh and Matveev 2009) (see Sec. 2). The periodic limit cycle trajectory of this model neuron overlaps the w-nullcline during the hyperpolarized phase of the oscillation, as shown in Figure 1. This feature of the periodic trajectory is explained by the strong time scale separation in the chosen parameter regime, with the w variable dynamics much faster than the V dynamics at hyperpolarized values of potential (see Fig. 1B). In this case a brief inhibitory input pushes the trajectory off the limit cycle, upon which the trajectory rapidly collapses to the w-nullcline, the slow manifold of the system. Thus, even after a perturbation is received, the trajectory of the model still lies close to a one-dimensional manifold, and we can describe the state of the model cell along the hyperpolarized branch of the w-nullcline using negative values of a one-dimensional phase variable, whereas its positive values on the cyclical domain $[0, 1]$ correspond to the unperturbed limit cycle. Figure 3 illustrates that this concept of negative phase follows naturally from the usual definition of phase in terms of normalized time to next spike. Namely, for phase-space points along the blue interval in Fig. 3A, the time to spike T_1 is greater than the resting spiking period, T_0 (see Fig. 3B). This leads to negative values of phase, given its usual definition as

$$\phi_n = 1 - \frac{T_1}{T_0} < 0 \tag{11}$$

According to this definition, the two phase space points on the same isochron in Fig. 1 will have two distinct values of phase: although the point on the limit cycle will have a phase value $0 < \phi'_{new} < 1$, the phase value at the point on the w-nullcline belonging to the same isochron will have a negative phase value $\phi_{new} = \phi'_{new} - 1 < 0$. This in fact is very convenient since the phase resetting $\Delta(\phi)$ can differ greatly at these two distinct points in phase space. Thus, extending the phase variable to include a negative value branch allows it to play dual roles of a temporal variable (isochron parameter) and a state-space variable (STRC argument) along a perturbed trajectory. It is important to note that negative phase parametrization of the perturbed trajectory requires that it should be transversal to a set of isochrons. This condition is automatically satisfied along the w nullcline, since it plays the role of the slow manifold, and therefore small displacement along this manifold results in large changes in time to spike.

Note however that certain distinct model states will be described by the same value of phase. This is true for a very narrow interval along the w-nullcline shown in magenta in Figure 3A, enclosed between the zero-phase isochron (grey curve), and the potential minimum V_{min} at the cusp of the limit cycle. Each point on this narrow interval will have the same small positive value of phase as a corresponding point along the downstroke of the action potential belonging to the same isochron, so both points will

Figure 3: Defining negative phase and extending phase response function to negative phase values. (A) Phase-space plot of the Morris-Lecar model (V vs. w) showing the limit cycle (bold black curve) and zero-phase isochron intersecting the peak of action potential (thin gray curve) (same as in Fig. 1). Negative phase values $\phi_n < 0$ correspond to points along the subthreshold branch of the w-nullcline to the left of its intersection with the zero-phase nullcline (blue line). Note a narrow interval of the w-nullcline shown in magenta for which phase is positive, since it is to the right of the $\phi = 0^-$ point. Hyperpolarizing pulse of amplitude δV shifts the phase-space point towards more negative phase values (red point). (B) Plot of voltage as a function of time. Trajectory with initial position at the blue point in panel A reaches peak of voltage at time $T_1 > T_0$ (blue curve), yielding negative phase values $\phi_n = 1 - T_1/T_0 < 0$, where T_0 is the intrinsic period of the cell. For the positive-phase interval shown in magenta in A, $T_1 < T_0$, and hence phase covers the same range as along the downstroke of the action potential. For any point with $\phi_n < 0$, phase resetting is defined as $\Delta(\phi_n) = (T_2 - T_1)/T_0$, where T_2 is the inter-spike interval perturbed by an inhibitory pulse or synaptic current received at phase ϕ_n (red curve).

Figure 4: Numerically generated STRC of the Morris-Lecar oscillator with type-I excitability, $\Delta(\phi)$, and its negative-phase extension, $\Delta_n(\phi)$. (A) First-order phase response to an inhibitory pulse current perturbation with $\delta V = -5mV$. (B) First-order (black and blue curves) and second-order (red curve) STRC corresponding to a synaptic current perturbation generated by a single presynaptic spike, with inhibitory synaptic conductance value of $\bar{g}_{syn} = 0.2$ mS/cm^2. In both panels, inset zooms into the interval of multi-valued STRC definition, $0 < \phi < 0.03$, where the lower branch ($\Delta(\phi)$, black curve) corresponds to the downstroke of the action potential, while the upper branch ($\Delta_n(\phi)$, bold blue curve) corresponds to the hyper-polarized interval of the w-nullcline shown in magenta in Fig. 3, and is a continuation of the negative-phase part of the STRC.

yield the same time to spike, slightly less than the unperturbed interval T_0. Because the amount of phase resetting at each of the two distinct phase space points will in general be different, the STRC we calculate below will have two branches on this narrow interval (see Fig. 4).

We are now ready to compute the phase response on the negative phase domain, as shown in Figure 3B. For any point corresponding to the negative phase $\phi_n < 0$, the phase response is defined as

$$\Delta_n(\phi_n) = \frac{T_2 - T_1}{T_0} \tag{12}$$

where T_2 is the time it takes for the potential to reach its peak following a hyperpolarizing pulse or a brief synaptic current, and T_1 is the corresponding first-passage time in the absence of perturbation, starting with hyperpolarized phase $\phi_n < 0$. In above, subscript "n" stands for negative; below we drop this subscript when describing phase resetting for both positive and negative phase values. We use numerical integration of the system ODEs to find the values of T_2, T_1 and T_0 needed to calculate the negative phases and their resetting values, given a certain value of perturbation or maximal synaptic conductance. Integration is carried out using MATLAB (see Methods), and quartic polynomial interpolation is used to reduce jitter in voltage peak detection.

Figure 4 demonstrates the resulting numerically generated phase response functions of the Morris-Lecar model for two different types of hyperpolarizing perturbations. Panel (A) of this figure shows the phase response to zero-width pulse current hyperpolarization (delta-function input current) with $\delta V = -5mV$, while Figure 4B is generated using continuous inhibitory current perturbation with $g_{syn} = 0.2$.

As mentioned above, phase response function is multi-branched on a narrow phase interval ($0 < \phi < 0.03$), which describes both the downstroke of the action potential, as well as points on the w-nullcline enclosed between the zero-phase isochron and the cusp of the periodic limit cycle (end of action potential). Note however that for continuous current perturbation (Fig. 4B), the difference between the two branches is relatively small, since the current duration is significantly larger than

Figure 5: Effect of three close synaptic inputs for strong value of the coupling, $\bar{g}_{syn} = 1.5$. The first synaptic input is applied at a fixed time of 0.3 ms (i.e $\phi_1 = 0.0367$) following the repolarization of the cell (i.e. following the minimum of voltage, $\phi = 0.0304$). The second synaptic input is applied $\Delta t_1 = 4$ ms after the first input, and arrives at phase $\phi_2 = \phi_1 - \Delta(\phi_1) + \Delta t_1/T_0 = -0.052$. The third synaptic input is applied $\Delta t_1 = 5$ ms after the second input, and arrives at phase $\phi_3 = \phi_2 - \Delta(\phi_2) + \Delta t_2/T_0 = -0.031$. The actual total phase delay due to all three inputs is measured as $\Delta_{total} = (T_3 - T_0)/T_0 = 0.3790$ where T_3 is the period perturbed by the combined application of all three inputs in one cycle of the oscillation (bold curve), and T_0 is the intrinsic period. This closely agrees with the sum of STRC values at phases $\phi_{1,2,3}$, which equals 0.3791.

the downstroke of the action potential, and therefore most of the input arrives while the cell is already on the slow manifold (w-nullcline). In contrast, in the case of the delta-function pulse-current perturbation the two branches do greatly differ, as to be expected given the phase-space separation between their domains. This however does not create any difficulties for phase delay prediction, since it is easy to check whether the action potential immediately preceded a given input, to determine which branch is to be used. Finally, note that the two branches satisfy continuity condition at their common point corresponding to the potential minimum, ϕ_{min}: $\Delta_n(\phi^-_{min}) = \Delta(\phi^+_{min})$, where $\Delta(\phi)$ and $\Delta_n(\phi)$ are the positive and negative-phase branches of the STRC, respectively.

Figure 4B also shows the second-order STRC (red curve), which describes the effect of perturbation received within one inter-spike interval on the duration of the following inter-spike interval (Canavier et al. 1997; Oprisan and Canavier, 2001; Oprisan et al. 2004). The second-order STRC is only non-zero if the input is received immediately before an action potential, since only in this case the input duration outlasts the time to nearest spike. Note that for purely pulsatile (zero-width) input, second order phase resetting is negligible, and is not shown. The second-order STRC, $\Delta_2(\phi)$, satisfies the continuity condition $\Delta_2(1^-) = \Delta(0^+)$ (Achuthan and Canavier, 2009).

Both phase response functions in Fig. 4 decrease to zero as the absolute value of negative phase increases, as one moves along the subthreshold branch of the w-nullcline in the negative V direction. This is similar to the case of the quadratic integrate-and-fire model shown in Fig. 2B, and reflects the fact that large negative phase values correspond to strongly hyperpolarized potentials, at which the relative effect of any additional inhibition becomes progressively smaller. We find that STRC is negligible below the phase value of about $\phi_0 = -0.2$ for $\bar{g}_{syn}$ up to 10 mS/ms^2; this negative phase value corresponds to membrane potential of around -500 mV.

3.3 Phase delay prediction for three close inputs using extended STRC

As discussed above, when the synaptic current is sufficiently strong and the time interval between two inputs is sufficiently small, the phase of the postsynaptic cell at the time of arrival of the second perturbation is negative. In this case the knowledge of the STRC on the negative phase domain is indispensable in order to describe the dynamics of the postsynaptic cell. Here we examine the dynamics of a single Morris-Lecar model neuron in response to three close synaptic inputs in the open-loop configuration, and test the accuracy of the spike time prediction based on the STRC extended to negative phase values, as shown in Fig. 5. The first synaptic input is applied at 0.3 ms following spike repolarization (potential minimum), corresponding to the phase of $\phi_1 = 0.037$. We fix the time interval between the first and second synaptic inputs at $\Delta t_1 = 4$ ms, while the interval between second and third synaptic inputs is fixed at $\Delta t_2 = 5$ ms.

Note that the time interval between two inputs is greater than the time of synaptic current decay, ensuring applicability and accuracy of the STRC approach. Given the synaptic decay time constant

Figure 6: Comparing the actual and the predicted combined phase delay produced by three successive synaptic inputs for a range of synaptic conductance values, 0.1 mS/cm^2 $< \bar{g}_{syn} <$ 2 mS/cm^2. Black open circles in top panel label the actual total inhibition measured by Eq. 13; red curve presents the total phase delay predicted using STRC extended to the negative phase domain (Eq. 14); **magenta line and asterisks mark the total phase delay obtained by replacing resetting at negative values of phase with its value at potential minimum, ϕ_{min}, using the STRC only defined in $[0, 1]$; the blue dashed curve and cross symbols show the total delay according to the "frozen" phase assumption ($\Delta_n(\phi_k < 0) = \Delta(\phi_{k-1})$).** Lower panel shows the value of phase at the time of arrival of the 2nd and 3rd synaptic inputs, for each value of $\bar{g}_{syn}$. Note that ϕ_2 is negative for $\bar{g}_{syn} > 0.2$ mS/cm^2, while ϕ_3 is negative when $\bar{g}_{syn} > 0.5$ mS/cm^2.

of 1 ms, and narrow width of the action potential, the synaptic current decays to less that 0.1% within about 4 ms. The second and third synaptic inputs arrive at phases ϕ_2, ϕ_3 given by Eqs. 9-10, where $T_0 = 44.96$ is the unperturbed period. The phase ϕ_2 at the time of arrival of the second synaptic input becomes negative when synaptic conductance satisfies $\bar{g}_{syn} > 0.2$ mS/cm^2, while the phase ϕ_3 at the time of arrival of the third input becomes negative when $\bar{g}_{syn} > 0.5$ mS/cm^2. In the example shown in Figure 5, $\bar{g}_{syn} = 1.5$, $\phi_2 = -0.052$ and $\phi_3 = -0.031$.

The actual total phase delay produced by the three synaptic inputs received at phases ϕ_1, ϕ_2 and ϕ_3 is measured as

$$\Delta_{total} = \frac{T_3 - T_0}{T_0} \tag{13}$$

where T_0 is the intrinsic period of the cell, and T_3 is the period prolonged by all three synaptic inputs arriving in one cycle (thick curve in Figure 5), computed by numerically integrating model equations. The phase delay at each phase is predicted using the numerically computed extended STRC as $\Delta(\phi_1)$, $\Delta(\phi_2)$ and $\Delta(\phi_3)$. Thus, we get the prediction

$$\Delta_{total} = \frac{T_3 - T_0}{T_0} \approx \Delta(\phi_1) + \Delta(\phi_2) + \Delta(\phi_3) \tag{14}$$

In the example shown in Figure 5, the actual total phase delay equals 0.3790, while $\Delta(\phi_1) + \Delta(\phi_2) + \Delta(\phi_3) = 0.1784 + 0.0898 + 0.1109 = 0.3791$.

In Figure 6 (top panel) we compare this prediction to the actual value of the perturbed delay for a range of synaptic conductance values, and show that the extended STRC gives a good approximation over the entire range of input strengths. As in Fig. 5, the first input is administered 0.3 ms after repolarization, while the intervals between the next two inputs are 4 ms and 5 ms, respectively. We compute the STRC for values of synaptic conductance $\bar{g}_{syn}$ from 0.1 to 2 mS/cm^2, and compare the actual value of the total delay obtained by numerically integrating the model equations with the value predicted from the phase map. Figure 6B shows that the values of phase at the time of arrival of the second and third inputs become progressively more negative as the synaptic conductance value increases. The phase delay prediction obtained using the STRC computed on the negative phase domain (red curve **in Fig. 6**) is compared with the following two alternative methods that one could reasonably consider in order to approximate the total delay without extending STRC to the negative phase domain:

1. Using STRC defined only on $[0, 1]$, with phase allowed to take on negative values upon hyperpolarization, but assuming that the value of resetting for negative values of phase equals the phase resetting at the phase corresponding to the minimum of potential, $\phi_{min} = 0.0304$: $\Delta_n(\phi < 0) = \Delta(0.0304)$ (magenta curve and asterisk symbols **in Fig. 6**). This method is described in Achuthan and Canavier (2009) and Achuthan and Canavier (2010).

Figure 7: Reconstructing the dynamics of an all-to-all inhibitory network of three ML cells, using iterative phase map based on the STRC extended to the negative phase domain, for $\bar{g}_{syn} = 0.15$. Top panel shows the potentials of the three cells versus time, obtained by numerical integration of model equations, while the bottom panel shows the spike sequence obtained using the iterative phase map described in Methods. For each triplet of spikes, the phase value of the first cell to spike is negative at the time of arrival of the third spike (phase values not shown). Initial cell phases are 0.25, 0.5 and 0.75. The error of spike time prediction gradually increases with simulation time, but remains within 1 ms for the entire spike sequence shown here.

2. Using STRC defined only on $[0, 1]$, and assuming that the phase of the cell is "frozen" by the first inhibitory input, e.g. $\Delta_n(\phi_2) = \Delta(\phi_1)$ when $\phi_2 < 0$ (blue dotted curve and cross symbols **in Fig. 6**).

Although one could also consider imposing the periodicity condition $\Delta_n(\phi < 0) = \Delta(1 - \phi)$, which would allow to avoid defining phase resetting at negative values of the argument, this method is the least accurate among those described, since such periodicity condition is arbitrary, and is not justified by the dynamical properties of the model; therefore, this method is not included in our comparison.

The three delay prediction methods only differ above $\bar{g}_{syn} < 0.2$ mS/cm^2, since below this value the cell phase is positive at the time of arrival of the two perturbations. Figure 6 shows that the negative phase STRC extension gives the best approximation among the three methods in the case of strong coupling strength. The absolute error between the actual total inhibition and the phase delay predicted using this approach remains within 0.3% over the entire range of $\bar{g}_{syn}$ that we used. The second-best method is that described in Achuthan and Canavier (2009), while the "frozen phase" method is the least accurate among the three. As to be expected, the latter two methods over-estimates the phase resetting for strong inhibitory inputs, since STRC decreases as the phase becomes negative (see Fig. 4). The lack of accuracy degradation of our extended STRC approach for very strong perturbations may be surprising, given relatively short separation between synaptic inputs of finite duration that we used here, but is explained by the decreasing sensitivity of time-to-spike with increasingly strong hyperpolarizations, noted above. This is also reflected in the gradual leveling off of the $\phi_{2,3}$ curves shown in the bottom panel of Fig. 6.

3.4 Phase delay prediction in a closed-loop circuit of three cells

While Fig. 6 shows the utility of the extended STRC in describing the response of a spiking model to perturbations in an open-loop configuration, it is important the examine the utility of this approach in a closed-loop circuit. In particular, a three-cell network gives a concrete example of the usefulness of extending the STRC to the negative phase domain, since in this case several synaptic inputs may arrive into each cell in each period of oscillation. In the example shown in Figure 7, we choose $\bar{g}_{syn} = 0.15$ mS/cm^2 for which the system has a stable splay state, so that each cell receives two consecutive synaptic inputs in every cycle. In this simulation, the phase of the cell that spikes first during each triplet is negative at the time of arrival of the second input within the same spike triplet. We apply the iterative phase map based on the STRC described in Methods to accurately predict the sequence of spikes in this case, which is shown in the bottom panel of Fig. 5.

Despite the excellent fidelity of the extended STRC approach in predicting network activity for small values of the coupling strength, it loses accuracy for larger values of $\bar{g}_{syn}$, due to the synchronizing effect of non-weak inhibition. As the time between afferent inputs becomes smaller, the main assumption of well-separated inputs at the basis of the STRC approach becomes violated, and the accuracy of spike prediction rapidly degrades. So even though the accuracy of phase delay prediction for each single

spike remains accurate, the appearance of closely-spaced spike doublets makes this method imprecise for synchronizing levels of inhibition. In this case accurate activity prediction is not possible without accounting for the non-linear interaction of close inputs.

4 Discussion

The extension of phase domain to the negative range arises naturally when deriving phase return maps in the case of non-weak inhibition, indicating the fact that upon sufficiently strong hyperpolarization the next spike is not expected sooner than after one intrinsic period has passed. This was first noted by Canavier and coworkers (Canavier et al 1999), who have subsequently applied STRC approach to describe complex activity states in networks of non-weakly coupled spiking cells such as splay states and other phase-locked states, which required extending the phase domain to negative values (Maran and Canavier, 2008; Canavier et al., 2009; Achuthan and Canavier, 2009; Canavier and Achuthan, 2010). In our recent work (Oh and Matveev, 2009) we examined the dynamic meaning of such negative phase domain in the particular case of the Morris-Lecar spiking model, and showed that the negative phase interval is associated with the nullcline of the recovery variable playing the role of the slow manifold of the system. However, the extension of the STRC to negative phase domain has not been considered in prior studies, and the value of STRC at negative phase values is usually replaced with an appropriate approximation (Achuthan and Canavier, 2009). Here we have shown that it is possible to avoid such approximations in some models with strong time-scale separation by defining the STRC on the negative domain, and demonstrated that such extension allows to more accurately describe the effect of non-weak inhibitory synaptic inputs in such models.

The existence of a uniquely-defined STRC at negative phase values (i.e. away from the limit cycle) suggests the existence of an approximate one-dimensional reduction of the dynamics in the corresponding part of phase space. Whereas in the weak-coupling limit such a one-dimensional reduction follows from the assumption of linearity and is achieved by the isochron foliation, for non-weak perturbations linearity does not hold and therefore an isochron does not uniquely determine the magnitude of the next phase resetting, which may vary significantly along any given isochron. As discussed above, in the Morris-Lecar model the relevant one-dimensional reduction is achieved because of rapid approach of all perturbed trajectories to the hyperpolarized segment of the recovery variable nullcline.

We presented the simplest illustration of the negative phase concept provided by the integrate-and-fire type models with a finite reset value, perturbed by hyperpolarizing inputs. In this case the values of potential between the reset and threshold values can be associated with a cyclic phase variable, whereas values of potential below reset represent a distinct branch of the state space, most conveniently defined using negative values of phase. This corresponds to the "tadpole"-like double-branch geometry of the one-dimensional state space of the integrate-and-fire model shown in Fig. 2A, first noted by Golubitsky et al. (2006). In fact, we have previously shown that the quadratic integrate-and-fire model exhibits stable leader-switching similar to that of the Morris-Lecar and Wang-Buzsáki models (Oh and Matveev, 2009), as should be expected given its connection to the canonical model of a type-I excitable cell (Ermentrout 1996).

One drawback of the negative phase extension of the STRC is the multivalued character of phase resetting on a narrow interval corresponding to the downstroke of the action potential. Along this segment of periodic trajectory the phase interval would have the same values as the narrow interval along the w-nullcline between the zero-phase isochron and the minimum of voltage, which are both represented by phase values slightly greater than zero. The value of phase resetting is very different

along these distinct one-dimensional manifolds, and therefore the value of STRC cannot be uniquely defined. However, this is not a significant concern since it is easy to determine which of the two branches is to be used, given the known time interval to preceding spike. Further, for time-dependent synaptic inputs, the difference between the two branches should be relatively insignificant.

Note that the negative phase description of strong perturbation is applicable to any model with pronounced time scale separation at hyperpolarized potentials, where the recovery currents activate quickly and where the membrane potential represents a single slow variable. In particular, this approach is not necessarily limited to type-I excitable cell models that we considered in this work. However, models with two or more slow variables may not be amenable to this description, unless hyperpolarizing inputs re-inject limit cycle points onto a one-dimensional curve within the slow manifold which is invariant, on slow time scales, with respect to potential perturbations.

Despite the high accuracy of the method in predicting the effect of an arbitrary number of successive perturbation, as well as activity of two-cell networks, its applicability to networks of more than two cells is limited by the fact that non-weak inhibition has a strongly synchronizing effect, leading to the possibility of simultaneously arriving inputs, and therefore violating the main assumption that the time interval between inputs should be longer than the duration of each synaptic input. Therefore, additional methods are required to improve the STRC method when dealing with inhibitory networks of more than two non-weakly coupled cells. For example, recently Achuthan and Canavier (2009) introduced a new approach to successfully tackle this situation, by re-computing the STRC for combinations of several simultaneous inputs. It would be interesting to investigate whether this method can be successfully combined with the extended STRC approach that we describe in this work. It is also important to explore whether the negative-phase STRC idea could be extended to **other biophysically inspired oscillator models**. We believe that further work in this direction could significantly contribute to the ongoing efforts in extending the phase resetting approach to non-weakly coupled networks, which is of value both for numerical simulation of network dynamics, as well as for rigorous analysis of emergent collective network activity states.

5 Acknowledgements

This research was supported in part by the National Science Foundation grant DMS-0817703 (V.M.).

References

[1] Achuthan S and Canavier CC (2009) *Phase-resetting curves determine synchronization, phase locking, and clustering in networks of neural oscillators.* J. Neurosci. 29:5218-5233.

[2] Acker CD, Kopell N, and White JA (2003) *Synchronization of Strongly Coupled Excitatory Neurons: Relating Network Behavior to Biophysics.* J. Comp. Neurosci. 15:71-90.

[3] Bartos M, Vida I, Geiger JRP and Jonas P (2001) *Rapid signaling at inhiitory synapses in a dentate gyrus interneuron network* J. of Neuroscience 21:2687-2698.

[4] Bressloff PC and Coombes S (2000) *Dynamics of strongly-coupled spiking neurons.* Neural Computation 12:91-129.

[5] Canavier CC, Butera RJ, Dror RO, Baxter DA, Clark JW, and Byrne JH (1997) *Phase response characteristics of model neurons determine which patterns are expressed in a ring circuit model of gait generation.* Biol. Cybernetics 77:367-380.

[6] Canavier CC, Baxter DA, Clark JW and Byrne JH (1999) *Control of multistability in ring circuits of oscillators.* Biol. Cybernetics 80:87-102.

[7] Canavier CC, Kazanci FG and Prinz AA (2009) *Phase resetting curves allow for simple and accurate prediction of robust N:1 phase locking for strongly coupled neural oscillators.* Biophys. J. 97:59-73.

[8] Canavier CC and Achuthan S (2010) *Pulse-coupled oscillators and the phase resetting curve.* Math. Biosci. 226:77-96.

[9] Dror RO, Canavier CC, Butera RJ, Clark JW and Byrne JH (1999) *A mathematical critereon based on the phase response curves for stability in a ring of coupled oscillators.* Biol. Cybern. 80:11-23.

[10] Ermentrout GB (1996) *Type I membranes, phase resetting curves, and synchrony.* Neural Computation 8:979-1001.

[11] Ermentrout GB and Kopell N (1984) *Frequency plateaus in a chain of weakly coupled oscillators.* SIAM J. Math. Anal. 15: 215-237.

[12] Ermentrout GB and Kopell N (1986) *Parabolic bursting in an excitable system coupled with a slow oscillation.* SIAM J. Applied Math. 46:233-253.

[13] Ermentrout GB and Kopell N (1990) *Oscillator death in systems of coupled neural oscillators.* SIAM J. Applied Math. 50:125-146.

[14] Ermentrout GB and Kopell N (1991) *Multiple pulse interactions and averaging in systems of coupled neural oscillators.* J. Math. Biol. 29:195-217.

[15] Goel P and Ermentrout GB (2002) *Synchrony, stability, and firing patterns in pulse-coupled oscillators.* Physica D. 163:191-216.

[16] Golubitsky M, Josic K and Shea-Brown E (2006) *Winding numbers and average frequencies in phase oscillator networks.* J. Nonlinear Sci. 16:201-231.

[17] Guckenheimer J (1975) *Isochrons and Phaseless Sets.* J. Math. Biol. 1: 259-273.

[18] Gutkin BS, Ermentrout GB, and Reyes AD (2005) *Phase-response curves give the responses of neurons to transient inputs.* J. Neurophys. 94:1623-1635.

[19] Hansel D, and Mato G (2003) *Asynchronous states and the emergence of synchrony in large networks of interacting excitatory and inhibitory neurons.* Neural Computation, 15:1-56.

[20] Hansel D, Mato G and Meunier C (1995) *Synchrony in excitatory neural networks.* Neural Computation 7:307-337.

[21] Izhikevich EM (2006) *Dynamics systems in neuroscience: The geometry of excitability and bursting.* Chapter 10: Synchronization. Cambridge, Massachusetts: MIT

[22] Izhikevich EM and Kuramoto Y (2006) *Weakly Coupled Oscillators.* Encyclopedia of Mathematical Physics, Elsevier, 5:448.

[23] Kuramoto Y (1984) *Chemical Oscillations, Waves, and Turbulence.* Springer, Berlin.

[24] Latham PE, Richmond BJ, Nelson PG, and Nirenberg S (2000). Intrinsic dynamics in neuronal networks. I. Theory. J. Neurophysiol. 83:808-827.

[25] Maran SK and Canavier CC (2008) *Using phase resetting to predict 1:1 and 2:2 locking in two neuron networks in which firing order is not always preserved.* J. of Comput. Nerosci. 24:37-55.

[26] Morris C, Lecar H (1981) *Voltage oscillations in the barnacle giant muscle fiber.* Biophys J 35: 193–213.

[27] Netoff TI, Banks MI, Dorval AD, Acker CD, Haas JS, Kopell N, and White JA (2005) *Synchronization in Hybrid Neuronal Networks of the Hippocampal Formation.*, J. Neurophysiol. 93:1197-1208.

[28] Oh M and Matveev V (2009) *Loss of phase-locking in non-weakly coupled inhibitory networks of type-I model neurons.* J. of Comput. Neurosci. 26(2):303-320.

[29] Oprisan SA, and Canavier CC (2001) Stability Analysis of Rings of Pulse-Coupled Oscillators: The Effect of Phase Resetting in the Second Cycle After the Pulse Is Important at Synchrony and For Long Pulses. J. Diff. Eq. and Dynamical Systems 9:243-258.

[30] Oprisan SA, Prinz AA, and Canavier CC (2004) *Phase resetting and phase locking in hybrid circuits of one model and one biological neuron.* Biophys. J. 87:2283-2298.

[31] Pfeuty B, Mato G, Golomb D, and Hansel D (2003) *Electrical synapses and synchrony: The role of intrinsic currents.* J. Neurosci. 23:6280-6294.

[32] Rinzel J and Ermentrout B (1998) *Analysis of Neural Excitability and Oscillations.* In: Methods in Neuronal Modeling: From Ions to Networks, 2nd edition, Eds. Koch C and Segev I. MIT Press, Cambridge, MA.

[33] van Vreeswijk C, Abbott LF, and Ermentrout B (1994) *When inhibition not excitation synchronizes neural firing.* J. of Comput. Neurosci. 1:313-321

[34] Winfree A. T. (1974) *Patterns of phase compromise in biological cycles.* J. Math Biol. 1: 73-95.

[35] Winfree A. T. (2001) *The Geometry of Biological Time,* 2nd edn. New York: Springer.

[36] Wang XJ, Buzsáki (1996) *Gamma oscillation by synaptic inhibition in a hippocampal interneuronal network model.* J. Neurosci. 16:6402-6413.

FIGURE LEGENDS

Figure 1. (A) Effect of two consecutive synaptic perturbations in the Morris-Lecar model. When one of the cells reaches phase 0, corresponding to the peak of its potential ($\phi_{pre} = 0$), a synaptic current hyperpolarizes the postsynaptic cell, which has phase ϕ_{old} immediately preceding the input. If this first synaptic input (green arrow) is sufficiently strong, the resulting phase delay is greater than the phase difference between the two cells (i.e. $\Delta(\phi_{old}) > \phi_{old}$), and the new phase will be negative, $\phi_{new} = \phi_{old} - \Delta(\phi_{old}) < 0$. This negative phase corresponds to an isochron that intersects the limit cycle at a position retrograde to the peak of the action potential (red curve). If the next synaptic input arrives immediately after the first one (red arrow), the phase of the postsynaptic cell will still be negative, and the resulting phase delay will require the knowledge of the STRC at this hyperpolarized part of the trajectory, $\Delta(\phi_{new})$. Note that the two points lying on the same red isochron have values of phase that differ by one oscillation cycle, $\phi_{new} = \phi'_{new} - 1$, so while ϕ'_{new} is positive (and close to 1), the phase ϕ_{new} is negative. (B) Time scale separation in the ML model. Contour plot shows the ratio of the membrane potential time constant (a function of V and w) to the time constant of K channel activation (a function of V only). Contours are labeled with the ratio value; note that this ratio is smaller than 0.02 at hyperpolarized potentials. A limit cycle is superimposed on the contour plot (blue curve).

Figure 2. Phase resetting at negative phase values in the quadratic integrate-and-fire model with reset potential $v_r = -1$. (A) Double-branch phase geometry of the model. Negative phase values correspond to values of potential below the reset. (B) Phase response curve given by Eq. 8, for a hyperpolarizing pulse of amplitude $\delta v = -7$. The portion of the curve corresponding to negative phase values is shown in bold. **Negative phase values are bounded from below by $\phi_0 = -1/3$, since the passage time from $v = -\infty$ to $v = v_r$ is finite and equals $T_0/3$ for the chosen value of v_r.** (C) Response of the model cell to three consecutive hyperpolarizing pulses of equal amplitude. The three inputs arrive at times 0.2, 0.5 and 0.9 following the spike. The resulting perturbed inter-spike interval is completely determined by the values of phase response at three values of phase $\phi_{1,2,3}$ indicated in B; summing them yields a phase delay of $0.363 + 0.136 + 0.168 = 0.667$. Given the unperturbed period of 2.356, this corresponds to a time delay of 1.57 shown in this panel. (D) The evolution of phase variable corresponding to voltage trace in C.

Figure 3. Defining negative phase and extending phase response function to negative phase values. (A) Phase-space plot of the Morris-Lecar model (V vs. w) showing the limit cycle (bold black curve) and zero-phase isochron intersecting the peak of action potential (thin gray curve) (same as in Fig. 1). Negative phase values $\phi_n < 0$ correspond to points along the subthreshold branch of the w-nullcline to the left of its intersection with the zero-phase nullcline (blue line). Note a narrow interval of the w-nullcline shown in magenta for which phase is positive, since it is to the right of the $\phi = 0^-$ point. Hyperpolarizing pulse of amplitude δV shifts the phase-space point towards more negative phase values (red point). (B) Plot of voltage as a function of time. Trajectory with initial position at the blue point in panel A reaches peak of voltage at time $T_1 > T_0$ (blue curve), yielding negative phase values $\phi_n = 1 - T_1/T_0 < 0$, where T_0 is the intrinsic period of the cell. For the positive-phase interval shown in magenta in A, $T_1 < T_0$, and hence phase covers the same range as along the downstroke of the action potential. For any point with $\phi_n < 0$, phase resetting is defined as $\Delta(\phi_n) = (T_2 - T_1)/T_0$, where T_2 is the inter-spike interval perturbed by an inhibitory pulse or synaptic current received at phase ϕ_n (red curve).

Figure 4. Numerically generated STRC of the Morris-Lecar oscillator with type-I excitability, $\Delta(\phi)$, and its negative-phase extension, $\Delta_n(\phi)$. (A) First-order phase response to an inhibitory pulse current perturbation with $\delta V = -5mV$. (B) First-order (black and blue curves) and second-order (red curve) STRC corresponding to a synaptic current perturbation generated by a single presynaptic spike, with inhibitory synaptic conductance value of $\bar{g}_{syn} = 0.2$ mS/cm^2. In both panels, inset zooms into the interval of multi-valued STRC definition, $0 < \phi < 0.03$, where the lower branch ($\Delta(\phi)$, black curve) corresponds to the downstroke of the action potential, while the upper branch ($\Delta_n(\phi)$, bold blue curve) corresponds to the hyper-polarized interval of the w-nullcline shown in magenta in Fig. 3, and is a continuation of the negative-phase part of the STRC.

Figure 5. Effect of three close synaptic inputs for strong value of the coupling, $\bar{g}_{syn} = 1.5$. The first synaptic input is applied at a fixed time of 0.3 ms (i.e $\phi_1 = 0.0367$) following the repolarization of the cell (i.e. following the minimum of voltage, $\phi = 0.0304$). The second synaptic input is applied $\Delta t_1 = 4$ ms after the first input, and arrives at phase $\phi_2 = \phi_1 - \Delta(\phi_1) + \Delta t_1/T_0 = -0.052$. The third synaptic input is applied $\Delta t_1 = 5$ ms after the second input, and arrives at phase $\phi_3 = \phi_2 - \Delta(\phi_2) + \Delta t_2/T_0 = -0.031$. The actual total phase delay due to all three inputs is measured as $\Delta_{total} = (T_3 - T_0)/T_0 = 0.3790$ where T_3 is the period perturbed by the combined application of all three inputs in one cycle of the oscillation (bold curve), and T_0 is the intrinsic period. This closely agrees with the sum of STRC values at phases $\phi_{1,2,3}$, which equals 0.3791.

Figure 6. Comparing the actual and the predicted combined phase delay produced by three successive synaptic inputs for a range of synaptic conductance values, 0.1 mS/cm^2 $< \bar{g}_{syn} <$ 2 mS/cm^2. Black open circles in top panel label the actual total inhibition measured by Eq. 13; red curve presents the total phase delay predicted using STRC extended to the negative phase domain (Eq. 14); **magenta line and asterisks mark the total phase delay obtained by replacing resetting at negative values of phase with its value at potential minimum, ϕ_{min}, using the STRC only defined in $[0, 1]$; the blue dashed curve and cross symbols show the total delay according to the "frozen" phase assumption ($\Delta_n(\phi_k < 0) = \Delta(\phi_{k-1})$)**. Lower panel shows the value of phase at the time of arrival of the 2nd and 3rd synaptic inputs, for each value of $\bar{g}_{syn}$. Note that ϕ_2 is negative for $\bar{g}_{syn} > 0.2$ mS/cm^2, while ϕ_3 is negative when $\bar{g}_{syn} > 0.5$ mS/cm^2.

Figure 7. Reconstructing the dynamics of an all-to-all inhibitory network of three ML cells, using iterative phase map based on the STRC extended to the negative phase domain, for $\bar{g}_{syn} = 0.15$. Top panel shows the potentials of the three cells versus time, obtained by numerical integration of model equations, while the bottom panel shows the spike sequence obtained using the iterative phase map described in Methods. For each triplet of spikes, the phase value of the first cell to spike is negative at the time of arrival of the third spike (phase values not shown). Initial cell phases are 0.25, 0.5 and 0.75. The error of spike time prediction gradually increases with simulation time, but remains within 1 ms for the entire spike sequence shown here.

lick here to download Figure: Fig1_revised.eps

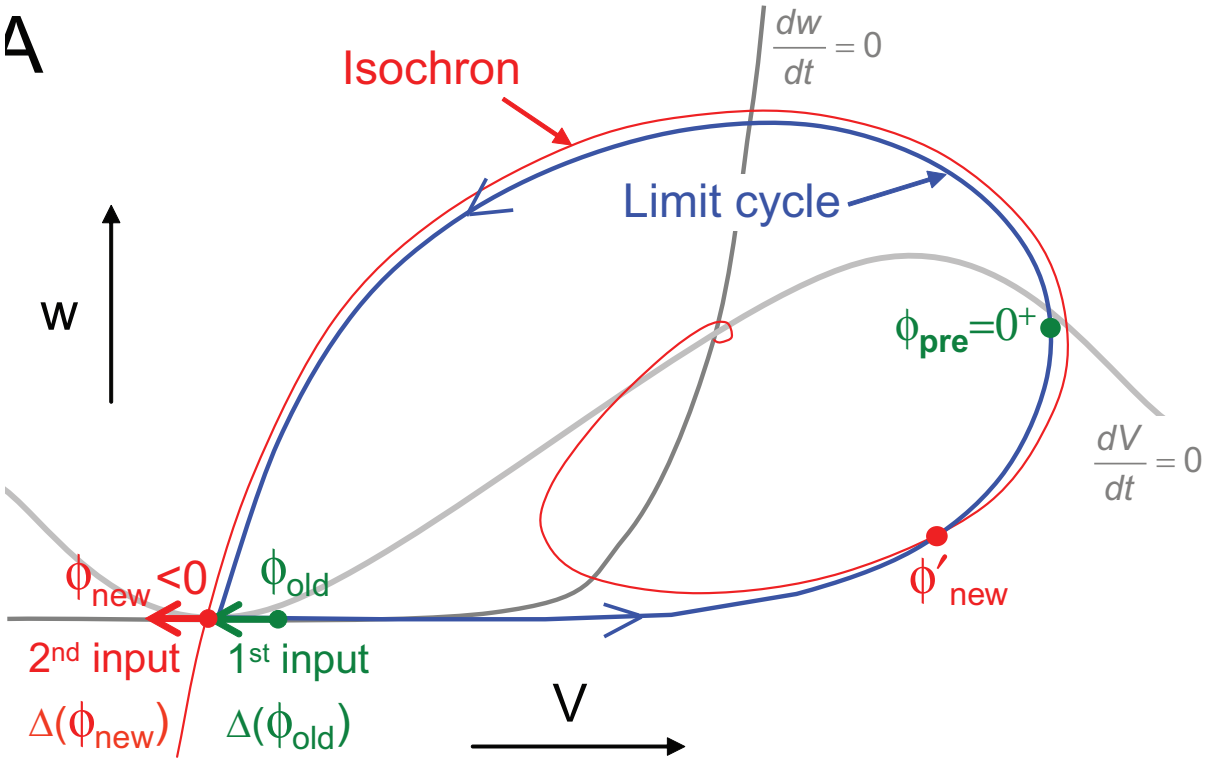

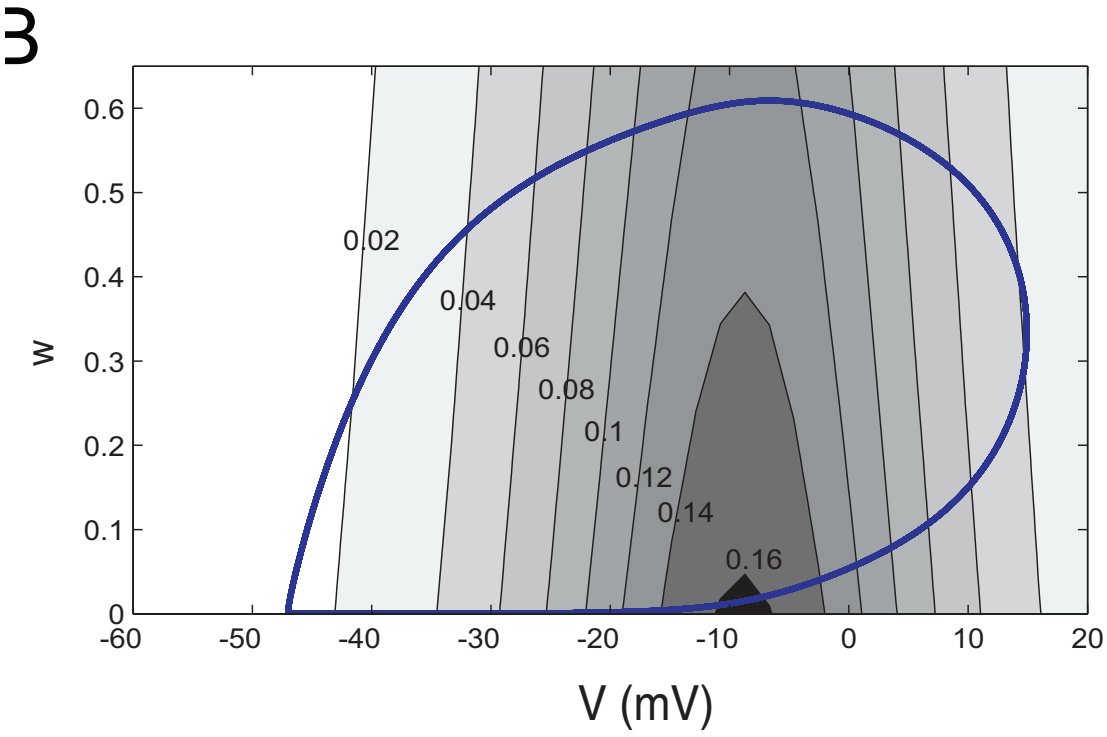

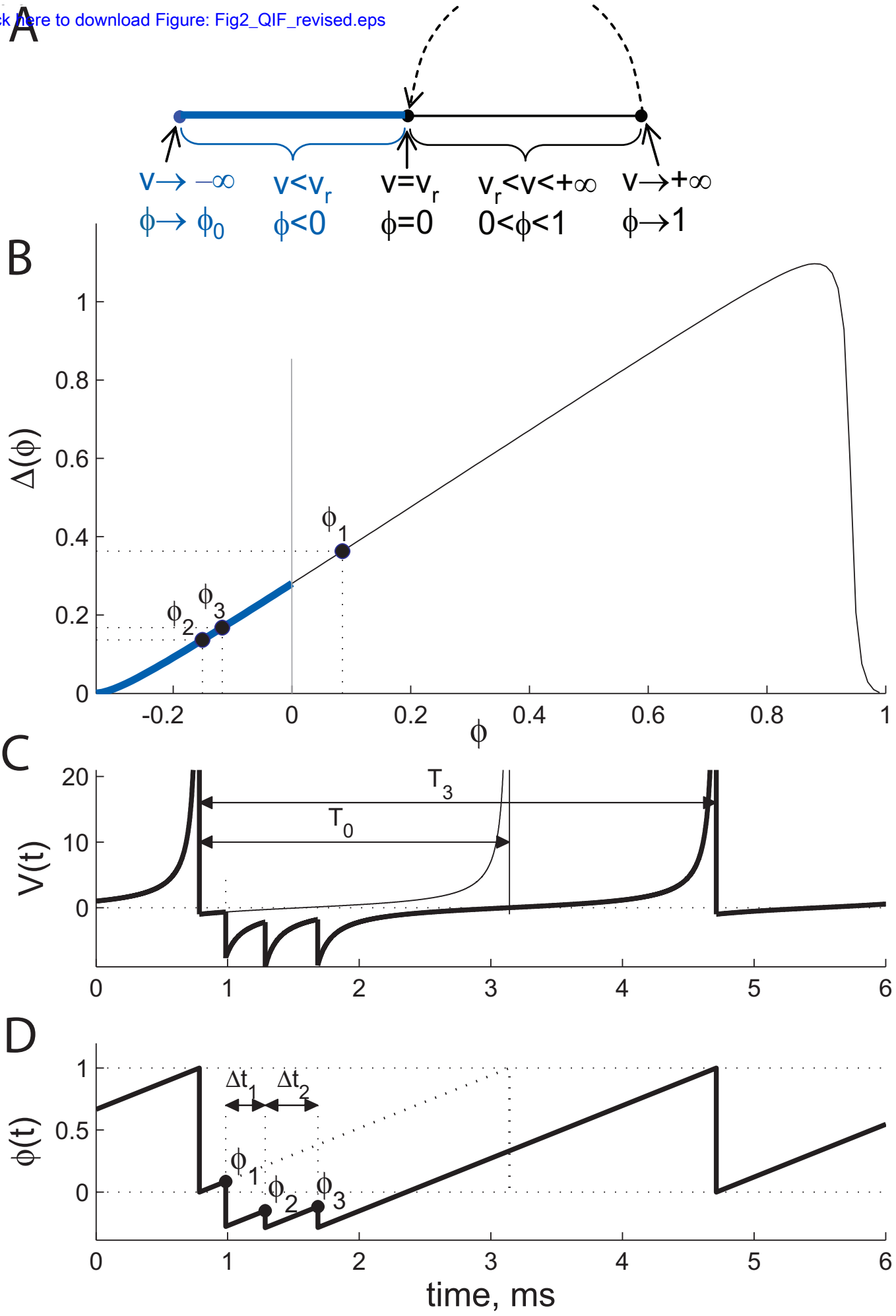

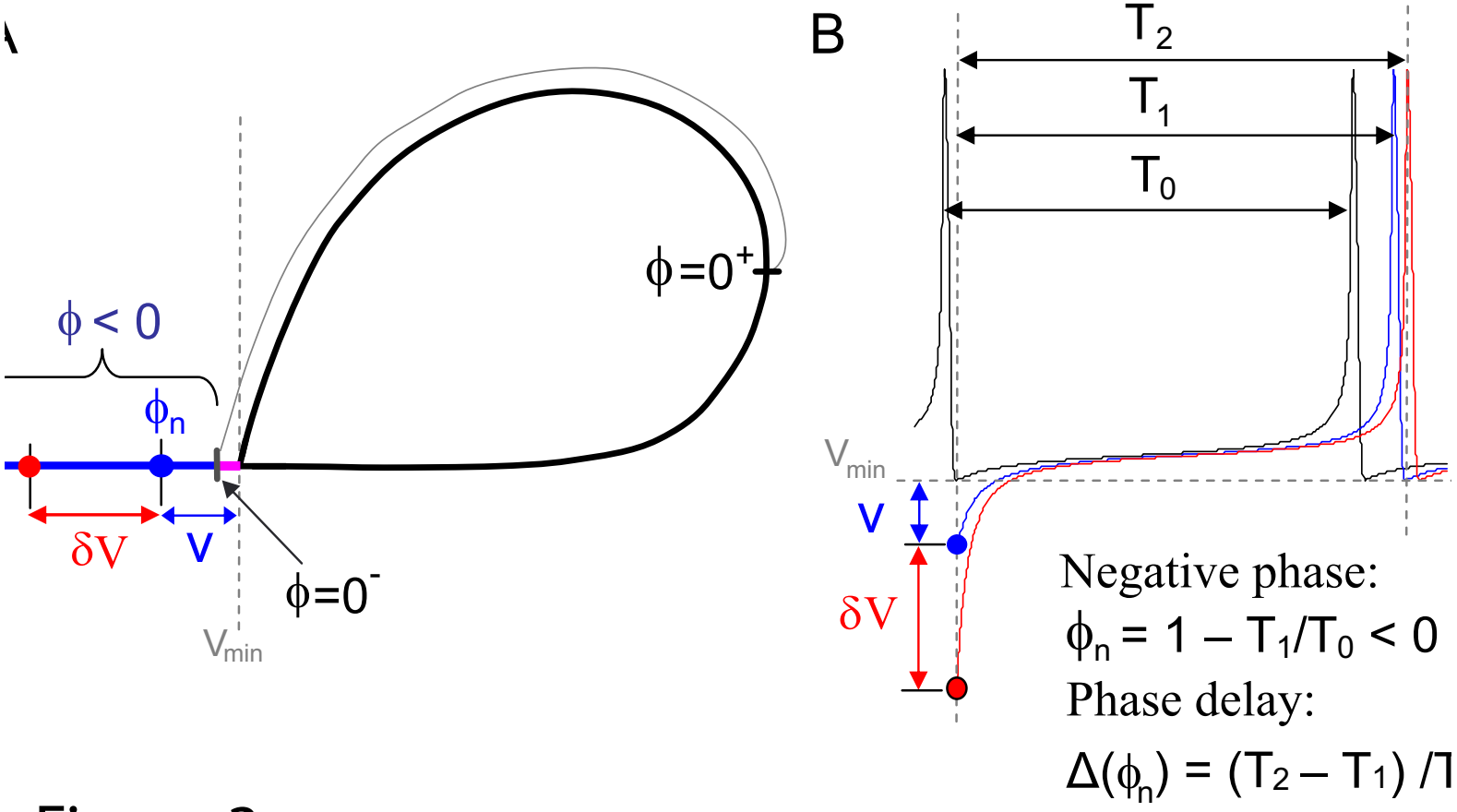

Figure 3

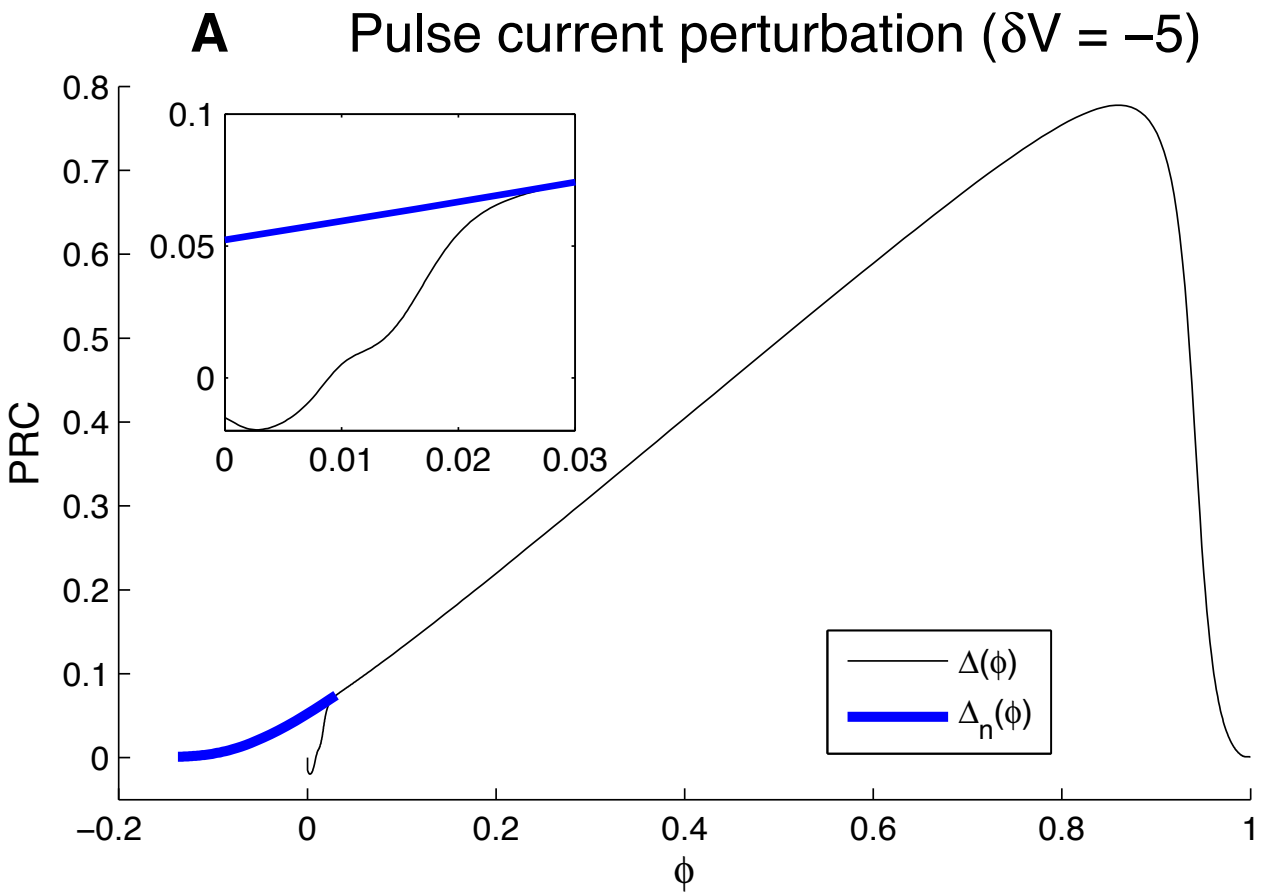

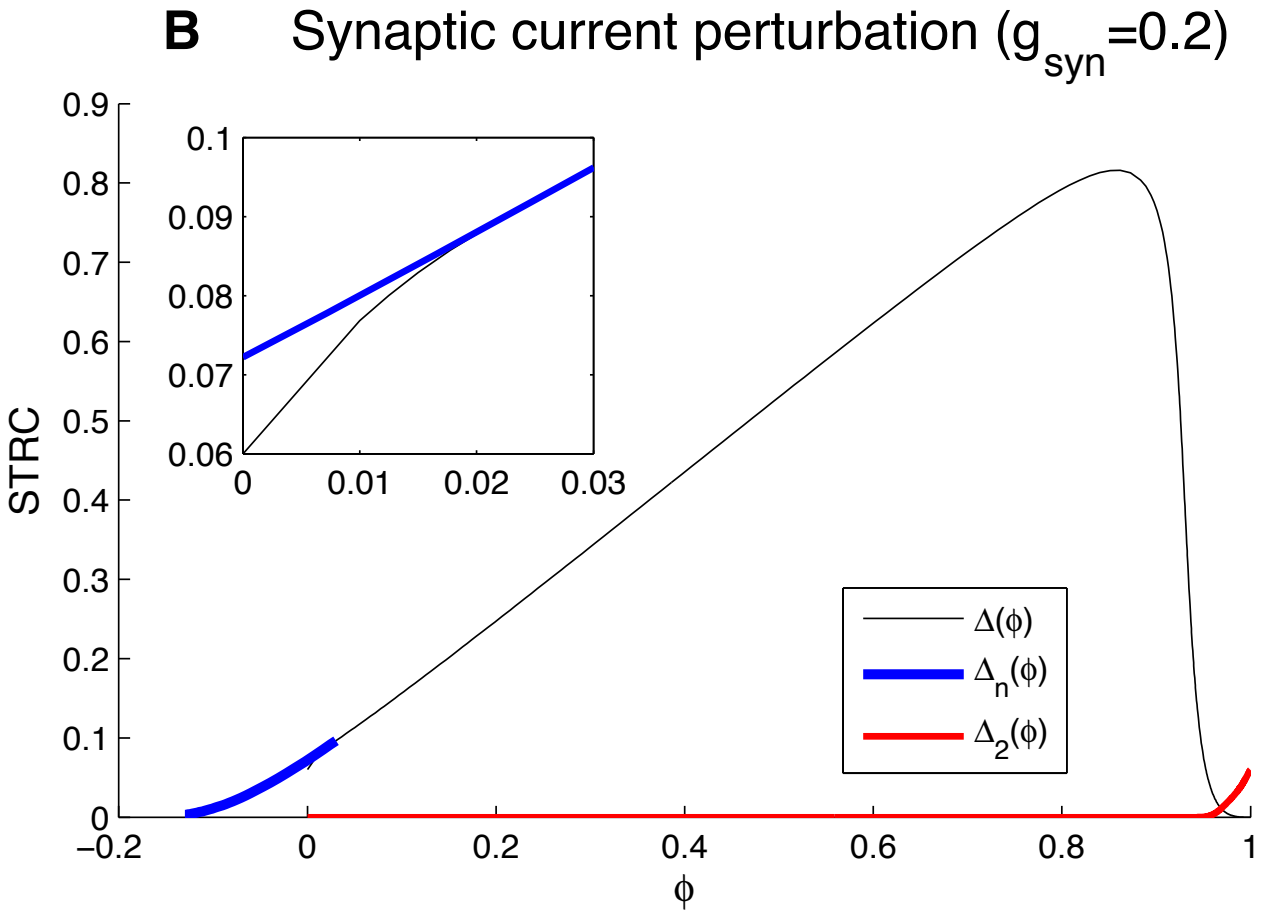

lick here to download Figure: Fig5_threePulse.eps

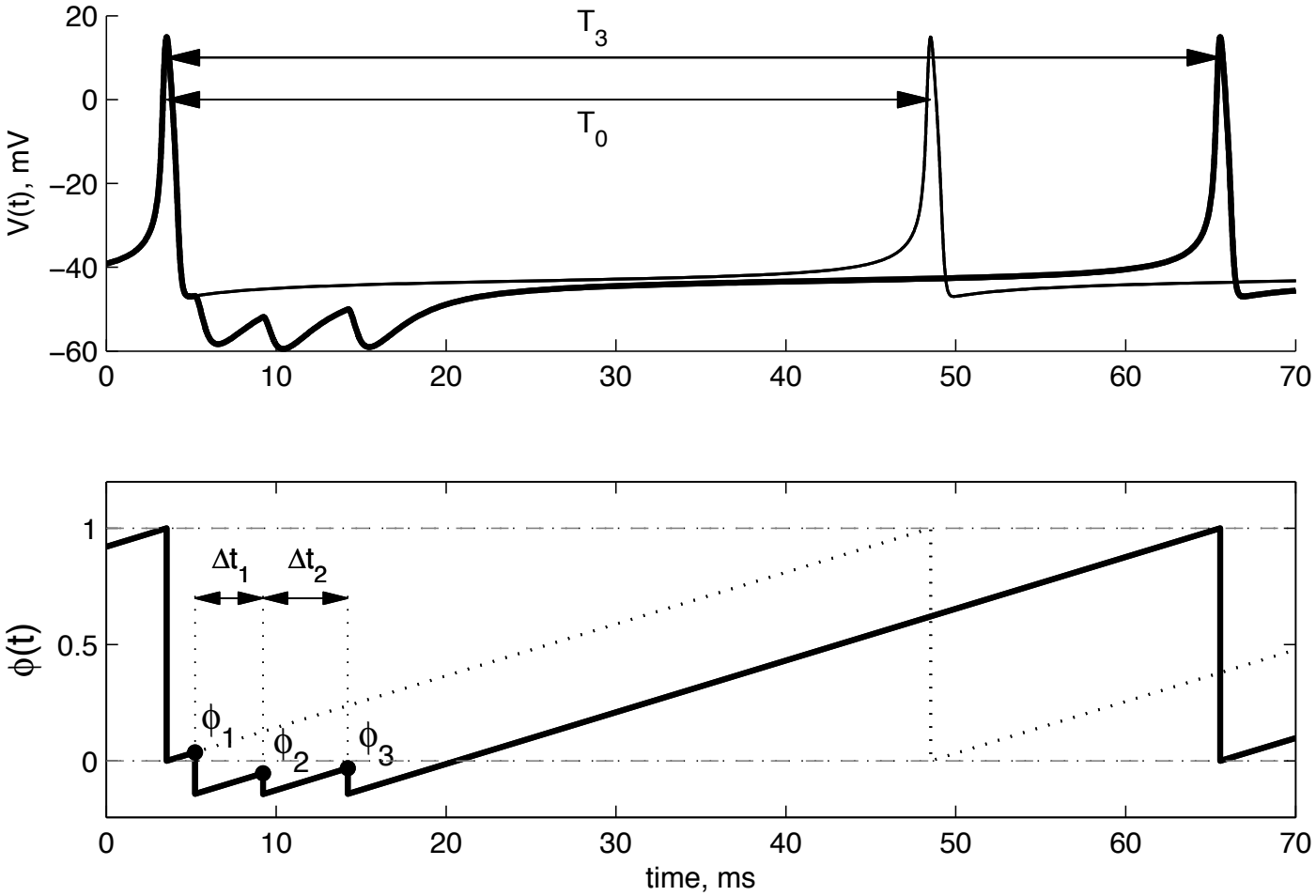

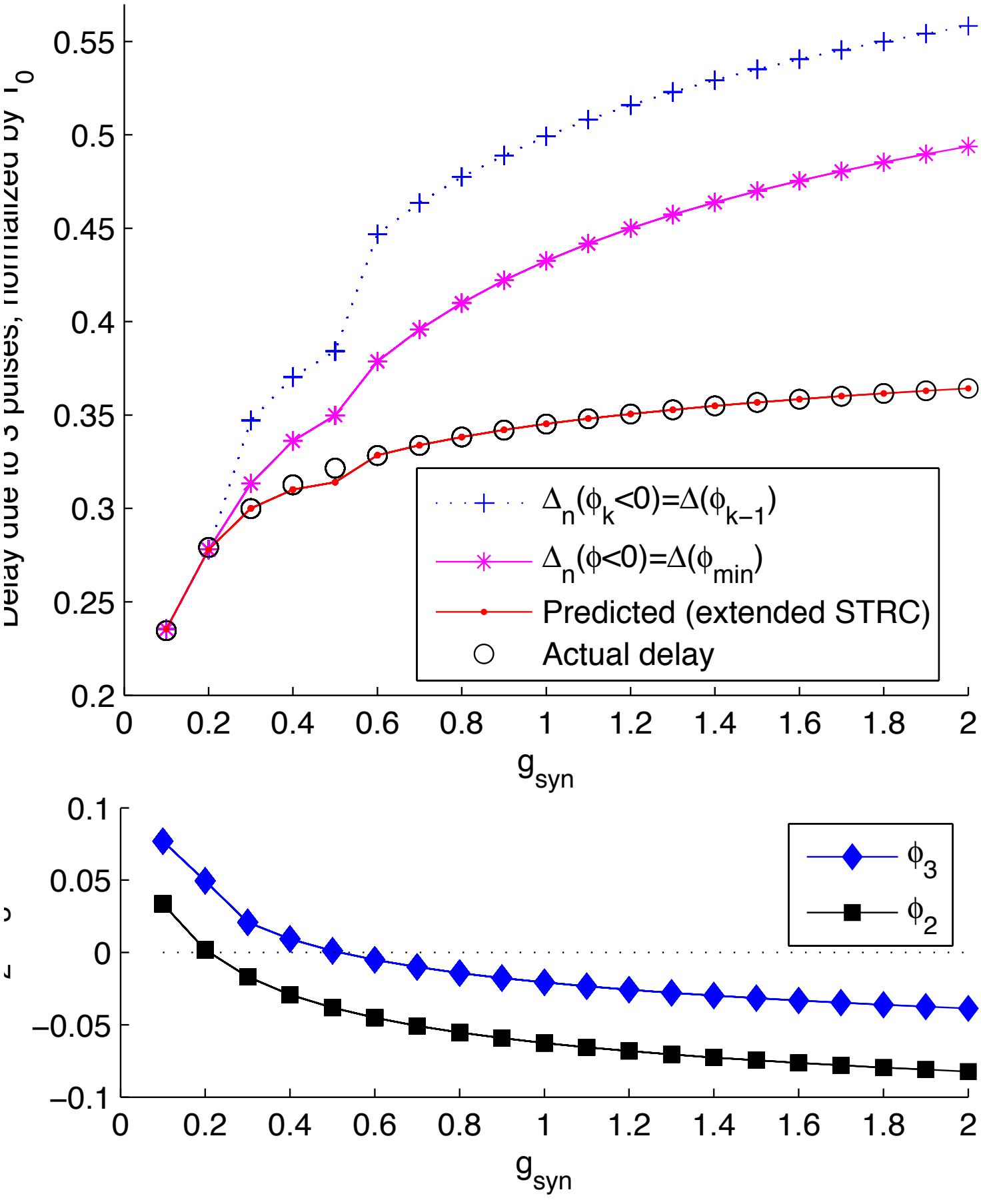

lick here to download Figure: Fig7_threeCell.eps